ELSEVIER

Nuclear Physics A 632 (1998) 275–284

NUCLEAR PHYSICS A

Cluster radioactivity and very asymmetric fission through compact and creviced shapes

G. Royer[a,1], Raj K. Gupta[b], V.Yu. Denisov[c]

[a] *Laboratoire Subatech, UMR: CNRS-Université-Ecole des Mines, 4 rue A. Kastler, 44307 Nantes Cedex 03, France*

[b] *Physics Department, Panjab University, Chandigarh-160014, India*

[c] *Institute for Nuclear Research, National Academy of Sciences of Ukraine, Kiev 252028, Ukraine*

Received 4 September 1997; revised 10 November 1997; accepted 8 December 1997

Abstract

The decay of radioactive nuclei which emit heavy clusters such as C, O, Ne, Mg and Si has been studied in the fission valley which leads one spherical nucleus towards two spherical touching nuclei before crossing the barrier. Assuming volume conservation, the macroscopic deformation energy has been calculated within a generalized liquid-drop model taking into account the proximity effects between the cluster and the daughter nucleus. The microscopic corrections have been introduced empirically to reproduce the experimental Q values. The theoretical partial half-lives obtained within the WKB barrier penetration probability are in good agreement with the experimental data. The C, O, Ne, Mg and Si emission looks like a spontaneous fission through very asymmetric compact and creviced shapes formed at the early stage of the tunneling process.

PACS: 23.70.+j; 21.10.Tg; 27.90.+b; 25.85.Ca
Keywords: Cluster radioactivity; Asymmetric fission; Half-lives; Liquid-drop model

1. Introduction

Experimentally, cluster radioactivity was discovered in 1984 [1]. In addition to the decay via α-particle emission, rare events of spontaneous decay of ^{223}Ra in a light ^{14}C fragment and a daughter ^{209}Pb nucleus was observed with a branching ratio to the α-emission of around 6×10^{-10} and a half-life of 2×10^{15} s. This new radioactivity

[1] Corresponding author. E-mail: royer@nanhp2.in2p3.fr.

0375-9474/98/$19.00
PII S0375-9474(97)00801-4

of heavy nuclei was predicted theoretically [2] in 1980 within the fragmentation theory [3,6] where the cold fusion and fission reaction paths appear naturally when the shell closure effects of one or both the reaction partners are taken into account.

Since this pioneering experiment, intense experimental activity has allowed the observation of the decay of 13 radioactive isotopes of Ra, Pa, U and Pu via the spontaneous emission of ^{14}C, ^{20}O, ^{23}F, ^{24,26}Ne, ^{28,30}Mg and ^{32}Si with branching ratios relative to α-decay from 10^{-9} down to 10^{-16} and partial half-lives from 10^{11} up to 10^{28} s [7,8]. The fine structure corresponding to branching ratios to the excited states of the daughter nucleus has also been observed [9,10] for ^{14}C decays of ^{222,223}Ra nuclei. A new possible island of cluster radioactivity around the doubly magic nucleus ^{100}Sn has recently been predicted [11–13]. A first preliminary investigation [14] has led to the selection of three possible events corresponding to the ^{12}C emission from ^{114}Ba; the final analysis concluding rather to the non-observation of this decay.

All the actually observed clusters are neutron-rich, even–even nuclei (except for ^{23}F) and not simply aggregates of α-particles. The daughter nucleus is an almost closed shell spherical nucleus. This points out the central role played by the shell and pairing effects in the selection of the possible emitted clusters.

The open question is whether both α and cluster decays correspond to the emission of a preformed cluster following the Gamow theory of α-decay while the spontaneous fission follows roughly the picture of the liquid-drop model or, alternatively, the α-decay, the heavy-ion emission and the spontaneous fission correspond to the same dynamical evolution of a nuclear liquid drop leading to two fragments but for three very different values of the asymmetry degree of freedom. In the approach of the preformed cluster models [15–17], the decay constant λ for cluster emission is the product of three terms: the barrier penetrability P, the assault frequency υ_0 and the cluster preformation probability P_0. The first contribution depends on the potential barrier while the last two vary with the size of the preformed cluster. In the approach of the unified fission models [18–20], cluster radioactivity is considered simply as a barrier penetration phenomenon and the decay constant is only the product of the barrier penetrability and of a constant assault frequency. Then, the position, width and height of the potential barriers are the main ingredients which determine the half-lives.

The purpose of the present work is to investigate an intermediate approach assuming that the cluster radioactivity is a very asymmetric fission process but also that this phenomenon occurs in the fusion-like second fission valley where the separation point between the two spherical nascent fragments is reached before negotiating of the barrier. This peculiar path through compact and creviced shapes and, later, two spherical body configurations seems plausible since, in this path: (i) the potential barrier heights are in agreement with the experimental symmetric and asymmetric fission and fusion barrier heights [21–24]; (ii) the Businaro–Gallone point is well reproduced [25]; and (iii) super and hyperdeformed states may survive at very high angular momenta [26].

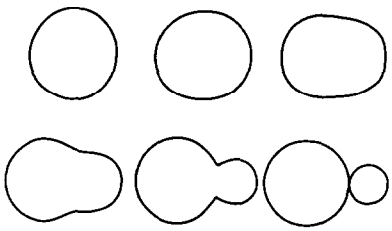

Fig. 1. Evolution of the shape leading from one spherical nucleus to two tangent spherical fragments of very different masses. The ratio between the transverse semi-axis (neck radius) and the highest fission semi-axis is, respectively, 1, 0.8, 0.6, 0.4, 0.2 and 0; the ratio between the radii of the nascent fragments is 0.46.

2. Very asymmetric fission model

The deformation path has been described within the one-parameter shape sequence already used to study asymmetric fusion [22] and fission [24]. Geometrically, the shape is defined from two different touching semi-elliptic lemniscatoids (Fig. 1). Volume conservation is assumed and the shape is axially symmetric. The formation of a deep neck occurs rapidly while the ends of the fissioning nucleus remain almost spherical. The dimensionless ratio between the neck radius and the largest elongation decreases from 1 for the spherical parent nucleus to 0 for the tangent spherical fragments and is a suitable parameter to define the shape for a given decay channel [22]. The volume, surface and moment of inertia are given by analytical formulae. The deformation parameter has been taken as the distance between the centres of mass of each nascent fragment. Its meaning is poor for one-body shapes within the fission picture. It has been calculated assuming that the future cluster and daughter nucleus are portions of lemniscatoids separated by a plane perpendicular to the fission axis. In this deformation valley, the later two separated spheres configuration also plays an essential role.

The potential energy is determined within the generalized liquid-drop model including the nuclear proximity effects [22]. For one-body shapes, the total energy is given by

$$E = -a_v(1 - k_v I^2)A + a_s(1 - k_s I^2)A^{2/3}(S/4\pi R_0^2) + \tfrac{3}{5}e^2\frac{Z^2}{R_0}B_c + E_{\text{prox}}, \qquad (1)$$

where A, Z and $I = (N - Z)/A$ are the mass, charge and relative neutron excess of the radioactive emitter, respectively. The surface and volume energy coefficients and the surface and volume asymmetry coefficients take on the values

$$a_s = 17.9439 \text{ MeV}, \qquad a_v = 15.494 \text{ MeV}, \qquad k_s = 2.6, \qquad k_v = 1.8. \qquad (2)$$

S is the surface of the deformed nucleus and B_c is the Coulomb shape-dependent function calculated from elliptic integrals.

The effective sharp radius of the parent nucleus is defined by

$$R_0 = 1.28A^{1/3} - 0.76 + 0.8A^{-1/3} \text{ fm}. \qquad (3)$$

In the first version of the liquid-drop model, the adopted value of $R_0/A^{1/3}$ was 1.2249 fm. Eq. (3) allows us to significantly lower the ratio $R_0/A^{1/3}$ and to reproduce its small increase with the mass. $R_0/A^{1/3}$ equals 1.10 fm for ^{14}C and 1.18 fm for ^{210}Pb.

When the two fragments are separated, the volume, surface and Coulomb energies are simply given by

$$E_v = -a_v[(1 - k_v I_1^2)A_1 + a_v(1 - k_v I_2^2)A_2], \tag{4}$$

$$E_s = a_s[(1 - k_s I_1^2)A_1^{2/3} + a_s(1 - k_s I_2^2)A_2^{2/3}], \tag{5}$$

$$E_c = \tfrac{3}{5}e^2 Z_1^2/R_1 + \tfrac{3}{5}e^2 Z_2^2/R_2 + e^2 Z_1 Z_2/r. \tag{6}$$

To ensure volume conservation, R_1 and R_2 read

$$R_1 = R_0(1 + \beta^3)^{-1/3} \text{ and } R_2 = R_0\beta(1 + \beta^3)^{-1/3}, \tag{7}$$

where

$$\beta = \frac{1.28A_2^{1/3} - 0.76 + 0.8A_2^{-1/3}}{1.28A_1^{1/3} - 0.76 + 0.8A_1^{-1/3}} \quad (A_2 < A_1). \tag{8}$$

The small energy gap appearing at the contact point due to the difference between A_1/Z_1 and A_2/Z_2 has been linearized from the contact point to the sphere since it originates from discarding the charge rearrangement in the nuclear matter which occurs progressively.

All along the fission path, the nuclear proximity energy, which takes into account the finite range effects of the nucleon–nucleon force inside the neck or the gap between the nascent or separated fragments, has been taken into account

$$E_{\text{prox}}(r) = 2\gamma \int_{h_{\min}}^{h_{\max}} \phi[D(r,h)/b]2\pi h\, dh, \tag{9}$$

where

$$\gamma = 0.9517\sqrt{(1 - k_s I_1^2)(1 - k_s I_2^2)} \text{ MeV fm}^{-2}, \tag{10}$$

h is the transverse distance varying from the neck radius or zero to the height of the neck border, D is the distance between the opposite infinitesimal surfaces, $b = 0.99$ fm is the surface width and ϕ the proximity function.

The validity of this prescription to determine the proximity energy has been confirmed with high accuracy for fusion data [22]. This additional term to the development of the liquid-drop model is not a small correction; it reaches, for example, −24 MeV at the contact point for $^{223}\text{Ra} \rightarrow {}^{14}\text{C} + {}^{209}\text{Pb}$ decay.

The parameter set of this generalized liquid-drop model has never been changed since the first fission and fusion studies [21,22]. Furthermore, no new adjustable parameter has been introduced to investigate the particular process of cluster emission.

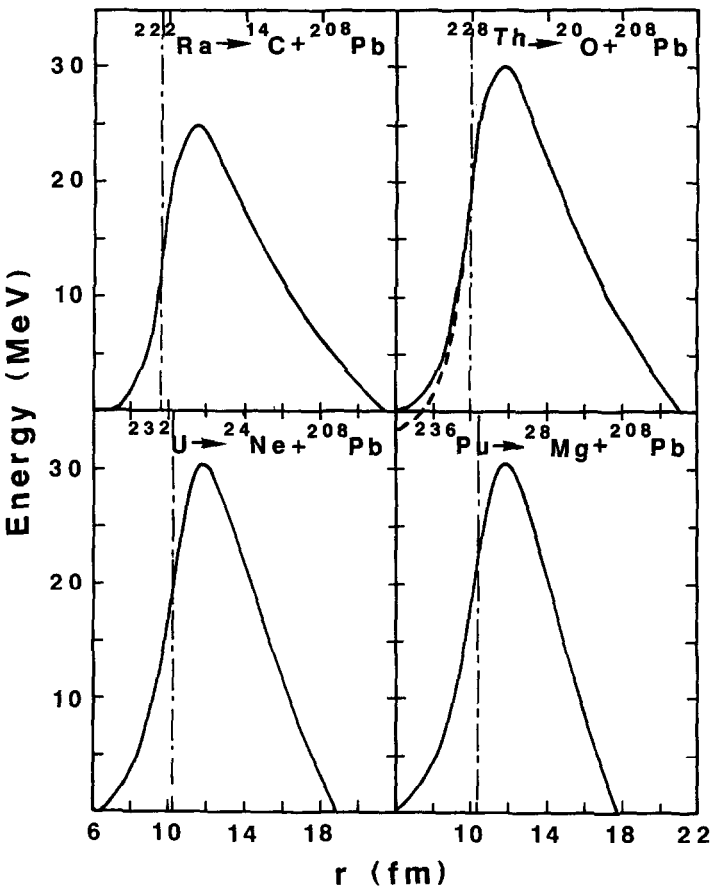

Fig. 2. Deformation energy including empirical microscopic corrections as a function of the centre-of-mass distance for four decays leading to the daughter nucleus ^{208}Pb. The vertical dashed and dotted line indicates the separation point between the spherical fragments. For ^{228}Th $\rightarrow$ ^{20}O + ^{208}Pb decay, the dashed curve corresponds to the macroscopic potential energy disregarding the microscopic corrections.

The microscopic corrections such as shell effects, pairing, etc. have been taken into account empirically. The difference between the experimental Q value and the theoretical Q value deduced from the present generalized LDM has been added at the macroscopic potential energy of the initial spherical nucleus with a linear attenuation factor vanishing at the contact point of the nascent fragments.

3. Potential barriers

As an illustration, in Fig. 2 four potential barriers are displayed for decays leading to light and heavy clusters and daughter nucleus ^{208}Pb. More generally, the geometrical and energetical theoretical characteristics are given in Tables 1 and 2 for the different cluster decay channels. The penetration of the barrier is considered to begin from Q_{EXP}

Table 1
Geometrical characteristics of the potential barriers for the different radioactive nuclei and emitted clusters. Both the macroscopic and microscopic contributions to the total energy are included. R_a and R_b are the inner and outer turning points. R_{cont} is the distance between the centres of the spherical cluster and daughter nucleus at the contact point. R_{bar} gives the position of the barrier top

Emitter and cluster	R_a (fm)	$R_{cont} = R_1 + R_2$ (fm)	R_{bar} (fm)	R_b (fm)
$^{222}Ra \rightarrow {}^{14}C + {}^{208}Pb$	6.5	9.7 = 2.7 + 7.0	11.5	21.6
$^{223}Ra \rightarrow {}^{14}C + {}^{209}Pb$	6.4	9.7 = 2.7 + 7.0	11.6	22.3
$^{224}Ra \rightarrow {}^{14}C + {}^{210}Pb$	6.3	9.7 = 2.7 + 7.0	11.6	23.2
$^{226}Ra \rightarrow {}^{14}C + {}^{212}Pb$	6.3	9.7 = 2.7 + 7.0	11.7	25.0
$^{228}Th \rightarrow {}^{20}O + {}^{208}Pb$	6.1	10.0 = 3.0 + 7.0	11.8	21.1
$^{230}Th \rightarrow {}^{24}Ne + {}^{206}Hg$	6.1	10.2 = 3.2 + 7.0	11.9	19.9
$^{231}Pa \rightarrow {}^{24}Ne + {}^{207}Tl$	6.1	10.2 = 3.2 + 7.0	11.9	19.3
$^{232}U \rightarrow {}^{24}Ne + {}^{208}Pb$	6.1	10.2 = 3.2 + 7.0	11.9	18.9
$^{233}U \rightarrow {}^{24}Ne + {}^{209}Pb$	6.1	10.3 = 3.25 + 7.05	11.9	19.5
$^{234}U \rightarrow {}^{24}Ne + {}^{210}Pb$	6.1	10.3 = 3.25 + 7.05	11.9	20.0
$^{234}U \rightarrow {}^{28}Mg + {}^{206}Hg$	6.1	10.4 = 3.4 + 7.0	12.0	18.7
$^{235}U \rightarrow {}^{28}Mg + {}^{207}Hg$	6.1	10.4 = 3.4 + 7.0	12.0	19.1
$^{236}Pu \rightarrow {}^{28}Mg + {}^{208}Pb$	6.1	10.4 = 3.4 + 7.0	12.0	17.7
$^{238}Pu \rightarrow {}^{28}Mg + {}^{210}Pb$	6.1	10.5 = 3.4 + 7.05	12.0	18.6
$^{238}Pu \rightarrow {}^{32}Si + {}^{206}Hg$	6.1	10.6 = 3.6 + 7.0	12.1	17.6

Table 2
Energetical characteristics (MeV) of the theoretical potential barriers including the macroscopic and microscopic contributions. E_{cont} and E_{bar} are, respectively, the energy at the contact point and at the top of the barrier relative to the energy of the spherical emitter nucleus. The Q_{LDM} value corresponds to the macroscopic energy of the parent nucleus relative to the macroscopic energy of the two infinitely separated fragments. Q_{EXP} gives the experimental value. Z_1Z_2 is the product of the fragment charges

Emitter and cluster	E_{cont}	E_{bar}	Q_{LDM}	Q_{EXP}	Z_1Z_2
$^{222}Ra \rightarrow {}^{14}C + {}^{208}Pb$	16.3	24.7	24.6	33.05	492
$^{223}Ra \rightarrow {}^{14}C + {}^{209}Pb$	17.4	25.7	24.4	31.84	492
$^{224}Ra \rightarrow {}^{14}C + {}^{210}Pb$	18.6	26.9	24.1	30.54	492
$^{226}Ra \rightarrow {}^{14}C + {}^{212}Pb$	20.9	29.1	23.7	28.20	492
$^{228}Th \rightarrow {}^{20}O + {}^{208}Pb$	21.9	30.3	43.2	44.73	656
$^{230}Th \rightarrow {}^{24}Ne + {}^{206}Hg$	24.9	32.8	58.0	57.65	800
$^{231}Pa \rightarrow {}^{24}Ne + {}^{207}Tl$	23.5	31.3	59.7	60.41	810
$^{232}U \rightarrow {}^{24}Ne + {}^{208}Pb$	22.7	30.5	61.4	62.31	820
$^{233}U \rightarrow {}^{24}Ne + {}^{209}Pb$	24.5	32.2	61.1	60.49	820
$^{234}U \rightarrow {}^{24}Ne + {}^{210}Pb$	26.1	33.8	60.8	58.83	820
$^{234}U \rightarrow {}^{28}Mg + {}^{206}Hg$	26.5	33.6	75.4	74.12	960
$^{235}U \rightarrow {}^{28}Mg + {}^{207}Hg$	28.2	35.4	74.9	72.16	960
$^{236}Pu \rightarrow {}^{28}Mg + {}^{208}Pb$	23.7	30.7	79.6	79.68	984
$^{238}Pu \rightarrow {}^{28}Mg + {}^{210}Pb$	27.2	34.2	78.8	75.92	984
$^{238}Pu \rightarrow {}^{32}Si + {}^{206}Hg$	27.0	33.4	92.8	91.20	1120

and the role of the difference between Q_{EXP} and Q_{LDM} is illustrated in Fig. 2 for $^{228}Th \rightarrow {}^{20}O + {}^{208}Pb$ decay.

Rupture of the neck occurs before reaching the position of the barrier top. The energy at the contact point of the spherical fragments varies from around 15 to 30 MeV above

the ground state of the parent nucleus. The potential barrier is mainly a scission barrier hindering neck formation and the separation process. The barrier top corresponds to two separated spherical fragments maintained in unstable equilibrium by the balance between the repulsive Coulomb forces and the attractive nuclear proximity forces. With increasing Coulomb repulsion, the length $R_b - R_a$ of the tunnel below the barrier diminishes slightly while the Q value increases. The barrier height (with respect to Q_{EXP}) varies from 30 to 35 MeV for the heavy cluster decays and from 25 to 30 MeV for the ^{14}C emission.

4. Theoretical and experimental half-lives

In such a unified fission model, the decay constant of the parent nucleus is simply defined as

$$\lambda = \upsilon_0 P. \tag{11}$$

There is no adjustable preformation factor. The assault frequency υ_0 can be evaluated from the zero point vibration energy $E_v = 1/2h\upsilon_0$ and, in the harmonic oscillator approximation [27],

$$\upsilon_0 = 2.5 \times 10^{20}\ \mathrm{s}^{-1}. \tag{12}$$

A detailed discussion on this value may be found in Ref. [7] (p. 375). In our approach, the nuclear shape is initially spherical and subsequently elongates. Consequently, the potential curves at smaller distances are not investigated.

The barrier penetrability P is calculated within the general form of the action integral

$$P = \exp\left\{-\frac{2}{\hbar}\int_{R_a}^{R_b}[2B(r)(E(r) - E(R_a))]^{1/2}\,dr\right\}, \tag{13}$$

with $E(R_a) = E(R_b) = Q_{EXP}$.

The expression proposed in Ref. [28] for the inertia $B(r)$ in this new fission valley has been used

$$B(r) = \mu\left\{1 + f(r)\tfrac{272}{15}\exp\left[-\tfrac{128}{51}((r - R_a)/R_0)\right]\right\}, \tag{14}$$

where

$$f(r) = \begin{cases} \left(\dfrac{R_{cont} - r}{R_{cont} - R_a}\right)^2, & r \leqslant R_{cont} \quad (R_{cont} = R_1 + R_2) \\ 0, & r \geqslant R_{cont} \end{cases}. \tag{15}$$

The partial half-life is related to the decay constant λ by

$$T_{1/2} = \frac{\ln 2}{\lambda}. \tag{16}$$

Table 3
Time characteristics (s) of the cluster radioactivity. The first and second columns indicate, respectively, the theoretical half-lives without and with taking into account the microscopic corrections. The last column gives the experimental data

Emitter and cluster	Theoretical $T_{1/2}$: macroscopic LDM barrier tunneling	Theoretical $T_{1/2}$: macroscopic and microscopic barrier tunneling	Experimental $T_{1/2}$
$^{222}Ra \rightarrow {}^{14}C + {}^{208}Pb$	2.7×10^{33}	2.0×10^{11}	1.2×10^{11}
$^{223}Ra \rightarrow {}^{14}C + {}^{209}Pb$	1.6×10^{34}	1.2×10^{14}	2.0×10^{15}
$^{224}Ra \rightarrow {}^{14}C + {}^{210}Pb$	1.1×10^{35}	1.9×10^{17}	7.4×10^{15}
$^{226}Ra \rightarrow {}^{14}C + {}^{212}Pb$	4.3×10^{35}	6.8×10^{22}	1.8×10^{21}
$^{228}Th \rightarrow {}^{20}O + {}^{208}Pb$	1.3×10^{26}	4.3×10^{22}	7.5×10^{20}
$^{230}Th \rightarrow {}^{24}Ne + {}^{206}Hg$	1.1×10^{26}	3.7×10^{26}	4.4×10^{24}
$^{231}Pa \rightarrow {}^{24}Ne + {}^{207}Tl$	2.9×10^{24}	1.2×10^{23}	1.7×10^{23}
$^{232}U \rightarrow {}^{24}Ne + {}^{208}Pb$	9.6×10^{22}	1.3×10^{21}	2.5×10^{20}
$^{233}U \rightarrow {}^{24}Ne + {}^{209}Pb$	3.3×10^{23}	4.7×10^{24}	6.8×10^{24}
$^{234}U \rightarrow {}^{24}Ne + {}^{210}Pb$	1.2×10^{24}	9.4×10^{27}	1.6×10^{25}
$^{234}U \rightarrow {}^{28}Mg + {}^{206}Hg$	7.6×10^{24}	1.4×10^{27}	3.5×10^{25}
$^{235}U \rightarrow {}^{28}Mg + {}^{207}Hg$	5.1×10^{25}	4.6×10^{30}	2.8×10^{28}
$^{236}Pu \rightarrow {}^{28}Mg + {}^{208}Pb$	2.0×10^{21}	1.7×10^{21}	4.7×10^{21}
$^{238}Pu \rightarrow {}^{28}Mg + {}^{210}Pb$	6.2×10^{22}	8.0×10^{27}	5.0×10^{25}
$^{238}Pu \rightarrow {}^{32}Si + {}^{206}Hg$	1.3×10^{25}	8.4×10^{27}	1.9×10^{25}

The theoretical and experimental partial half-lives are compared in Table 3. The macroscopic part of the total energy leads to a reasonable agreement for the heaviest clusters but fails to reproduce the ^{20}O and ^{14}C emission. In contrast, when the microscopic contributions are included, our theoretical estimates agree very well with the data for all the C, O, Ne, Mg and Si clusters. Therefore, it seems that the emission of clusters by heavy nuclei may be viewed as the limiting case of very asymmetric fission via compact and creviced shapes.

The differences to other works which have also reproduced the experimental data must be underlined. In the preformed cluster models [7,15–17], the clusters are assumed to be pre-born in the parent nucleus before they can penetrate the potential barrier with a given Q value and the cluster preformation probability P_0 as well as the barrier assault frequency υ_0 depend strongly on the size of the clusters. For example, P_0 can reach 10^{-10}. In the asymmetric fission models, $P_0 = 1$ and υ_0 is generally independent on the cluster size.

The unified fission models differ mainly in the derivation of the potentials and the selected shape sequences. Contrary to our description within a generalized liquid-drop model assuming constant density during the fission process, most of the approaches use empirical and fitted analytical expressions to calculate the potential energy. In the analytical super-asymmetric fission model [18], the potential is approximated by a second-order polynomial in the separation distance between two intersected spheres up to the touching configuration and, later, for separated spheres, the interacting potential is simply the Coulomb potential. In Ref. [19] a simple power law describes the potential before the touching configuration while a nuclear proximity potential is added to the

Coulomb repulsion when the fragments are separated. The combination of a third-order polynomial before the contact point with a Yukawa-plus-exponential potential and a Coulomb potential after the contact point has also been used [29].

5. Conclusion

The decay of radioactive nuclei which emit heavy clusters such as C, O, Ne, Mg and Si has been studied in the fusion-like second fission valley which leads from one spherical nucleus to two spherical touching nuclei before negotiating the barrier. Assuming volume conservation, the deformation energy has been calculated within a generalized liquid-drop model taking into account the proximity effects between the cluster and the daughter nucleus. The microscopic corrections to the total energy have been estimated and introduced from the difference between the experimental Q value and that given by the macroscopic generalized liquid-drop model. The partial half-lives obtained within the WKB penetration probability are in very good agreement for all the emitted clusters. Therefore, the emission of C, O, Ne, Mg and Si nuclei can be described within a spontaneous tunneling process under the fusion-like second fission valley.

It is important to emphasize that the main explanation for the good reproduction of the experimental data is the ability of the present model to reproduce the height and width of the potential barriers with the help of the experimental Q value. The physical process which leads to two tangent spherical fragments may be an adiabatic fission process or, alternatively, the emission of a preformed cluster. Whatever the physical process, the roles of the microscopic corrections and the proximity energy are emphasized since their introduction allows us to reproduce the potential barrier characteristics which govern the half-lives.

Acknowledgements

Two of us (RKG and VYD) are thankful for the support from the French Institut National de Physique Nucléaire et de Physique des Particules and Ecole des Mines de Nantes.

References

[1] H.J. Rose and G.A. Jones, Nature 307 (1984) 245.
[2] A. Sandulescu, D.N. Poenaru and W. Greiner, Sov. J. Part. Nucl. 11 (1980) 528.
[3] H.J. Fink, W. Greiner, R.K. Gupta, S. Liran, H.J. Maruhn, W. Scheid and O. Zohni, in: Int. Conf. on Reactions between Complex Nuclei, Nashville, 1974, eds. R.L. Robinson et al. (North-Holland, Amsterdam, 1975) p. 21.
[4] A. Sandulescu, R.K. Gupta, W. Scheid and W. Greiner, Phys. Lett. B 60 (1976) 225.
[5] R.K. Gupta, A. Sandulescu and W. Greiner, Phys. Lett. B 67 (1977) 257.
[6] R.K. Gupta, S. Gulati, S.S. Malik and R. Sultana, J. Phys. G 13 (1987) L27.
[7] R.K. Gupta and W. Greiner, Int. J. Mod. Phys. E 3 (1994) 335.

[8] Yu.S. Zamyatnin, V.L. Mikheev, S.P. Tret'yakova, V.I. Furman, S.G. Kadmenskii and Yu.M. Chuvil'skii, Sov. J. Part. Nucl. 21 (1990) 231.
[9] M. Hussonnois, J.F. LeDu, L. Brillard, J. Dalmasso and G. Ardisson, Phys. Rev. C 43 (1991) 2599.
[10] R. Bonetti, C. Chiesa, A. Guglielmetti, C. Migliorino, P. Monti, A.L. Pasinetti and H.L. Ravn, Nucl. Phys. A 576 (1994) 21.
[11] S. Kumar, D. Bir and R.K. Gupta, Phys. Rev. C 51 (1995) 1762.
[12] D.N. Poenaru, W. Greiner and E. Hourani, Phys. Rev. C 51 (1995) 594.
[13] G. Shanmugam, G.M. Carmel Vigila Bai and B. Kamalaharan, Phys. Rev. C 51 (1995) 2616.
[14] A. Guglielmetti, R. Bonetti, G. Poli, P.B. Price, A.J. Westphal, Z. Janas, H. Keller, R. Kirchner, O. Klepper, A. Piechaczek, E. Roeckl, K. Schmidt, A. Plochocki, J. Szerypo and B. Blanck, Phys. Rev. C 52 (1995) 740.
[15] R. Blendowske, T. Fliessbach and H. Walliser, Nucl. Phys. A 464 (1987) 75.
[16] S.S. Malik and R.K. Gupta, Phys. Rev. C 39 (1989) 1992.
[17] S. Kumar, R.K. Gupta and W. Scheid, Int. J. Mod. Phys. E 3 (1994) 195.
[18] D.N. Poenaru, M. Ivascu, A. Sandulescu and W. Greiner, Phys. Rev. C 32 (1985) 572.
[19] Y.J. Shi and W.J. Swiatecki, Nucl. Phys. A 464 (1987) 205.
[20] F. Barranco, G.F. Bertsch, R.A. Broglia and E. Vigezzi, Nucl. Phys. A 512 (1990) 253.
[21] G. Royer and B. Remaud, J. Phys. G 10 (1984) 1057.
[22] G. Royer and B. Remaud, Nucl. Phys. A 444 (1985) 477.
[23] G. Royer, J. Phys. G 12 (1986) 623.
[24] G. Royer and F. Haddad, Phys. Rev. C 51 (1995) 2813.
[25] F. Haddad and G. Royer, J. Phys. G 21 (1995) 1357.
[26] G. Royer and F. Haddad, Phys. Rev. C 47 (1993) 1302.
[27] C. Wagemans, The Nuclear Fission Process (CRC Press, Boca Raton, FL, 1991) p. 36.
[28] P. Möller, J.R. Nix and W.J. Swiatecki, Nucl. Phys. A 492 (1989) 349.
[29] G. Shanmugam and B. Kamalaharan, Phys. Rev. C 38 (1988) 1377.